1 **Chitosan/carrageenan nanoparticles: Effect of cross-linking with tripolyphosphate**

2 **and charge ratios**

3 *Susana Rodrigues[1], Ana M. Rosa da Costa[2], Ana Grenha[1*]*

4 [1]CBME – Centre for Molecular and Structural Biomedicine / IBB – Institute for

5 Biotechnology and Bioengineering, University of Algarve, Faculty of Sciences and

6 Technology, Campus de Gambelas, 8005-139 Faro, Portugal: [2]CIQA – Centre of

7 Research in Chemistry of Algarve, Faculty of Sciences and Technology, Campus de

8 Gambelas, 8005-139 Faro, Portugal

9

10

11

12 *Corresponding author:

13 *E-mail address:* amgrenha@ualg.pt

14 *Postal address:* Centre for Molecular and Structural Biomedicine (CBME), Faculty of

15 Sciences and Technology, Building 8, Room 2.4, Campus de Gambelas, 8005-139 Faro,

16 Portugal

17 *Phone:* +351 289800100 - Ext. 7441

18 *Fax:* +351 289 818419

19

20 **ABSTRACT**

21 Chitosan/carrageenan/tripolyphosphate nanoparticles were prepared by polyelectrolyte

22 complexation/ ionic gelation, the latter compound acting as cross-linker. The

23 incorporation of the three components in the nanoparticle matrix was assessed by

24 analytical techniques (FTIR, XPS and TOF-SIMS).

25 Using chitosan/carrageenan nanoparticles as control, the effect of the cross-linker in the

26 particles properties was studied. A decrease in size (from 450-500 nm to 150-300 nm)

27 and in zeta potential (from +75 - +85 mV to +50 - +60 mV), and an increase in

28 production yield (from 15-20% to 25-35%), and in stability (from one week to up to 9

29 months) were observed. Also, a correlation between positive to negative charge ratios in

30 the formulations and the above characteristics was established.

31 The small size and high positive surface charge make the developed

32 chitosan/carrageenan/tripolyphosphate nanoparticles potential tools for an application in

33 mucosal delivery of macromolecules.

34

35 **Keywords:** chitosan, cross-linking, *k*-carrageenan, nanoparticles, tripolyphosphate

36

1.   Introduction

Polymeric nanoparticles have been used increasingly in various fields, such as drug

delivery, imaging and tissue engineering, the first being, by far, the most reported

application. The main reason justifying the widespread use of polymeric nanoparticles

relies on the displayed high surface-to-volume ratio which improves the loading

capacity of the selected molecule, while providing its protection. In addition, increased

drug absorption might be attained by the capacity of nanoparticles to reduce epithelial

resistance to transport (de la Fuente, Csaba, Garcia-Fuentes & Alonso, 2008; Rawat,

Singh & Saraf, 2006; Reis & Ribeiro, 2006).

Many polymers have been used to prepare these vehicles, but those of natural origin are

often preferred because, as compared to synthetic counterparts, they comply more easily

with the requisites of biocompatibility, biodegradability and absence of toxicity that are

mandatory in any biomedical application (Liu, Jiao, Wang, Zhou & Zhang, 2008;

Malafaya, Silva & Reis, 2007). Chitosan (CS) and carrageenan (CRG) are two marine-

derived polymers which belong to the above mentioned class, and have demonstrated in

a previous study the ability to assemble into nanoparticles of 400-600 nm (Grenha et al.,

2010). CS is a cationic polysaccharide composed of repeating units of *N*-

acetylglucosamine and D-glucosamine that are β-(1-4)-linked (Figure 1), and presents

well-documented favorable properties for drug delivery such as biocompatibility,

biodegradability, low toxicity (Dornish, Hagen, Hansson, Peucheur, Vedier &

Skaugrud, 1997; Hirano, Seino, Akiyama & Nonaka, 1988) and mucoadhesiveness

(Lehr, Bouwstra, Schacht & Junginger, 1992). CRG is another polysaccharide, extracted

from red seaweed (van de Velde, Knutsen, Usov, Rollemay & Cerezo, 2002) and

composed of galactose and anhydrogalactose units, linked by glycosidic bonds (Figure

1) (Lim, Gwon, Choi, Shin & Nho, 2010). Due to its half-ester sulfate moieties,

62 carrageenan displays a strong ionic nature and exhibits a high capacity to react with

63 proteins (Malafaya, Silva & Reis, 2007; Mohamadnia, Zohuriaan-Mehr, Kabiri,

64 Jamshidi & Mobedi, 2007). There are two types of carrageenan that evidence gel-

65 forming ability, *k-* and *i-*, *k*-carrageenan gels being more firm than those obtained with *i-*

66 carrageenan, which are more elastic and soft (Bixler, 1993). The assembly of the

67 referred CS/CRG nanoparticles was mediated by polyelectrolyte complexation (Grenha

68 et al., 2010), a method that uses very mild conditions, avoiding harmful organic solvents

69 or high shear forces. Therefore, it has the general capability of protecting the

70 encapsulated molecules and retaining their activity during the encapsulation, which are

71 its principal advantages (Mohanraj & Chen, 2006; Saboktakin, Tabatabaie, Maharramov

72 & Ramazanov, 2010; Grenha, 2012). This methodology involves the interaction

73 between a chitosan with high degree of protonation and a polyanion, permitting the

74 rapid formation of nanoparticles. Their size, as well as other characteristics, might be

75 modulated by adjusting formulation parameters like the type of materials composing the

76 particles matrix, their concentration and mass ratios, amongst others (Calvo et al. 1997a;

77 Grenha, 2012).

78 In many cases, for instance if the nanoparticles are to be applied in mucosal delivery, it

79 is important to ensure that their size will permit the contact with the epithelial surface,

80 an effect that is maximised for particles between 50 and 500 nm (Desai, Labhasetwar,

81 Amidon & Levy, 1996; Jani, Halbert, Langridge & Florence, 1990). Preparing

82 nanoparticles in this size range is facilitated by the use of adequate cross-linking agents.

83 Tripolyphosphate (TPP) is a non-toxic polyanion (Figure 1) known for its capacity to

84 cross-link chitosan, a reaction mediated by electrostatic forces, resulting in the

85 formation of ionic cross-linked networks (Janes, Calvo & Alonso, 2001; Mi, Sung,

86 Shyu, Su & Peng, 2003).

The objective of this work was to produce CS/CRG nanoparticles, including in the formulation TPP as cross-linking agent, and to evaluate the effect of the presence of this polyanion on the properties of nanoparticles, namely concerning size, surface charge and stability. To do so, different amounts of cross-linker were used and formulations with different polymeric mass ratios were tested. Reduced size and strong positive surface charge would improve the nanoparticles contact with mucosal epithelial surfaces, which is very positive when considering an application in mucosal drug delivery.

2.   Experimental

2.1. Materials

Chitosan (low molecular weight, deacetylation degree = 75-85%), pentasodium tripolyphosphate, glycerol and glacial acetic acid were supplied by Sigma Chemicals (Germany). k-carrageenan and potassium bromide (KBr) were obtained from FMC Biopolymer (Norway) and Riedel-del-Haën (Germany), respectively. Ultrapure water (Milli-Q Plus, Millipore Iberica, Spain) was used throughout.

2.2. Nanoparticles preparation

CS/CRG/TPP nanoparticles were prepared by a modification of a previously described methodology (Grenha et al., 2010), based on the polyelectrolyte complexation of CS with CRG and additional ionic gelation of chitosan with TPP anions. Briefly, CS was dissolved in 1% (w/w) acetic acid to obtain a solution of 1 mg/mL and CRG and TPP were dissolved in purified water to obtain stock solutions of 2.5 and 1.0 mg/mL, respectively. Different volumes of the latter solutions were mixed in order to obtain volumes of 0.8 mL of solutions with the required concentrations of both components.

112   The spontaneous formation of nanoparticles occurs upon incorporation, under gentle

113   magnetic stirring at room temperature, of the aforementioned solutions into 2 mL of the

114   CS solution, corresponding to final theoretical CS/CRG/TPP ratios varying from 4/1/0

115   to 7/1/1 (w/w).

116   Nanoparticles were concentrated by centrifugation at 16 000 x g on a 10 µL glycerol

117   layer for 30 min at 15 °C (centrifuge 5804R, Eppendorf, Germany). The supernatants

118   were discarded and nanoparticles were ressuspended in 200 µL of purified water.

119

120   **2.3. Nanoparticles physicochemical characterization**

121   The production yield of nanoparticles was calculated by gravimetry. Fixed volumes

122   of nanoparticle suspensions were centrifuged (16 000 x g, 30 min, 15 °C), and

123   sediments were freeze-dried over 24 h at -34 °C, followed by a gradual increase in

124   temperature until 20 °C, using a Labconco freeze dryer (Labconco, USA) ($n = 3$).

125   The process yield (P.Y.) was calculated as follows: P.Y. (%) = (nanoparticle

126   sediment weight/total solid weight) x 100.

127   The morphological examination of CS/CRG/TPP nanoparticles was conducted by

128   transmission electron microscopy (TEM) (JEM-1011, JEOL, Japan). The samples were

129   stained with 2% (w/v) phosphotungstic acid and placed on copper grids with Formvar[®]

130   films for TEM observation.

131   Measurements of nanoparticle size and zeta potential were performed on freshly

132   prepared samples by photon correlation spectroscopy and laser Doppler anemometry,

133   respectively, using a Zetasizer Nano ZS (Malvern Instruments, Malvern, UK). For the

134   analysis of particle size and determination of the electrophoretic mobility, each sample

135   was diluted to the appropriate concentration with ultrapure water and placed in the

6

136   electrophoretic cell. Each analysis was performed at 25 °C. Three batches of each

137   formulation were analyzed ($n = 3$).

138

139   **2.4. Nanoparticle stability study**

140   Aliquots of nanoparticle formulations with and without TPP (formulations 5/1/1 and

141   5/1/0, respectively) were stored at 4 ºC. Nanoparticle sizes and zeta potentials were

142   monitored as a function of time for 250 days, using the technique described above ($n =$

143   3).

144

145   **2.5. Nanoparticles chemical analysis**

146   *2.5.1. Fourier transform infrared (FTIR) spectroscopy*

147   The interactions between the different components of the nanoparticulate systems

148   were analyzed by FTIR. Infrared spectra of the specimen powders, namely CS, CRG

149   and TPP, and CS/CRG/TPP nanoparticles (formulation 5/1/1), were recorded using a

150   FTIR spectrophotometer (Tensor 27, Bruker, Germany). Prior to the assay, the samples

151   were gently triturated with KBr and compressed into discs.

152   For each spectrum a 32-scan interferogram was collected in transmittance mode with

153   a 4 cm^{-1} resolution in the 4000–400 cm^{-1} region at room temperature.

154

155   *2.5.2. Surface analysis by X-Ray photoelectron spectroscopy (XPS) and time-of-*

156   *flight secondary ion mass spectrometry (TOF-SIMS)*

157   The surface of CS/CRG/TPP nanoparticles was analyzed to determine their chemical

158   composition. To do so, a droplet of nanoparticles (formulations 4/1/1 and 5/1/1) was

159   placed directly on a polished monocrystalline silicon wafer, used as a sample holder.

160   The droplet was then allowed to dry in a desiccator, prior to the analyses. The surface of

161   the samples was analyzed by XPS (K-Alpha ESCA, Thermo Scientific, UK) and TOF-

162   SIMS (TOF-SIMS IV, Ion-TOF GmbH, Germany). Solutions of the different

163   compounds (CS, CRG and TPP) were analysed separately as controls.

164   The XPS measurements were carried out using monochromatic Al-Ka radiation ($hv =$

165   1486.6 eV), and photoelectrons were collected from a take-off angle of 90° relative to

166   the sample surface. The X-Ray monochromatic spots were 400 μm in diameter and the

167   correspondingly sampling area was 0.1256 mm^2. Measurements were performed in

168   constant analyzer energy (CAE) mode with 100 eV pass energy for survey spectra and

169   20 eV pass energy for high-resolution spectra. Charge referencing was done by setting

170   the lower binding energy C 1s photopeak at 285.0 eV, the C 1s hydrocarbon peak

171   (Briggs & Seah, 1983). Surface elemental composition was determined using the

172   standard Scofield photoemission cross section. Residual vacuum in the analysis

173   chamber was maintained at around 3 x 10^{-9} mbar.

174   For TOF-SIMS analyses, samples were bombarded with a pulsed bismuth ion beam

175   (Bi^{3+}) generated with a liquid metal ion gun operated at 25 keV and a 45° incidence

176   with respect to the sample surface. The secondary ions generated were extracted with a

177   10 kV voltage, and their time-of-flight from the sample to the detector was measured in

178   a reflectron mass spectrometer. Electron flood gun charge compensation was necessary

179   during measurements. A raster size of 500 μm × 500 μm was used, and at least three

180   different spots were analyzed under the "static" condition with ion doses of 2 x 10^{12}

181   ions/cm^2. The calibration of the mass spectra in the positive mode was based on

182   hydrocarbon peaks such as CH_3^+, $C_2H_3^+$, $C_3H_5^+$ and $C_7H_7^+$. Negative spectra were

183   calibrated to the C^-, C_2^-, C_3^-, C_4^-, C_2H^-, C_3H^- and C_4H^- peaks before further analysis. The

184   experimental conditions (ion type, beam voltage, and primary ion dose) were

185   maintained constant for each experiment.

186

2.6. Statistical analysis

The t-test and the one-way analysis of variance (ANOVA) with the pair wise

multiple comparison procedures (Student-Newman-Kleus Method) were performed to

compare two or multiple groups, respectively. All analyses were run using the

SigmaStat statistical program (Version 3.5, SyStat, USA) and differences were

considered to be significant at a level of $p < 0.05$.

3.   Results and discussion

3.1. CS/CRG/TPP nanoparticles characterization

CS/CRG/TPP nanoparticles were produced by a very mild polyelectrolyte

complexation/ionic gelation method, as described in the Experimental Section. Briefly,

when the three components are mixed, an electrostatic interaction is established between

the positively charged amino groups of CS and the negatively charged sulphate and

phosphate groups of CRG and TPP, respectively, leading to the nanoparticle formation

in a process derived from inter- and intramolecular linkages mediated by the anionic

molecules (Janes, Calvo & Alonso, 2001). TPP affords a further intense interaction, as it

provides a cross-linking effect. Figure 2 displays a TEM microphotograph of

representative CS/CRG/TPP nanoparticles, showing a spherical morphology and

compact structure.

An estimation of the positive to negative (+/-) charge ratios for the different

formulations was made, based on the following assumptions: 1) Chitosan was

considered to have one positive charge per deacetylated monomer and, since it has a

deacetylation degree of 75-85%, a mean value of 0.8 positive charges per monomer was

used. According to a reported method (Ma et al, 2008) an average monomeric molecular

weight of 169 g/mol for this deacetylation degree was obtained; 2) Carrageenan was assumed to be in the sodium salt form, to which corresponds a mass of 408 g/mol and a negative charge per disaccharide monomer unit; 3) Pentasodium tripolyphosphate has a molar mass of 368 g/mol and five negative charges per anion. The mass of each compound in every formulation was then converted to moles of charge and the +/- molar ratio was calculated.

As can be seen in Figure 3, formulations with mass ratios below 4/1/1 (as 2/1/0.5 and 3/1/1), which evidence a +/- charge ratio around 1 (Figure 3A), resulted in precipitation (Figure 3B). The observed precipitation for lower ratios is due to the presence of an excess of anionic charges, which neutralize chitosan positive charges and, thus, reduce or eliminate electrostatic repulsion, leading to precipitation. In fact, a 1:1 +/- charge stoichiometry does not mean that complete charge neutralization will occur, due to different charge spacings in the intervenient species and to steric constraints. However, one may assume a preferential interaction between the sulphate and the ammonium groups, both weakly hydrated, instead of with the strongly hydrated counterions (Crouzier & Picart, 2009). The same assumption should apply to TPP polyanion. This would lead to mainly an intrinsic charge matching in detriment of an extrinsic charge compensation and, thus, to a small deviation from neutrality.

On the contrary, the formulation corresponding to a mass ratio of 7/1/0, which displays a +/- charge ratio of 13.5, did not lead to nanoparticle formation. As observed by other authors and, according to the described formation mechanism of nanoparticles, which is mediated by electrostatic interactions, the absence of nanoparticle formation is attributed to an insufficient number of anionic charges to neutralise CS amino groups (Calvo, Remuñán-López, Vila-Jato & Alonso, 1997a; Fernández-Urrusuno, Calvo, Remuñán-López, Vila-Jato & José Alonso, 1999). For this reason, Figure 4 only depicts

236   the physicochemical characteristics of CS/CRG/TPP nanoparticles of mass ratios

237   between 4/1/0 and 6/1/1.

238   Observing in Figure 4A the data corresponding to formulations containing only

239   CS/CRG (4/1/0 to 6/1/0), no significant differences are observed for both size and zeta

240   potential, which lay around 450-500 nm and +80 mV, respectively. However, bearing in

241   mind the observations of Figure 3A, concerning charge ratios, there is a tendency to

242   decrease the size from the formulation 4/1/0 (charge ratio of 7.7) to 6/1/0 (charge ratio

243   of 11.6), which is attributed to the increase in the charge ratio, as reported elsewhere

244   (Chen, Mohanraj, Wang & Benson, 2007; Nizri, Magdassi, Schmidt, Cohen & Talmon,

245   2004; Nizri, Makarsky, Magdassi & Talmon, 2009). Increasing CRG content in the

246   formulation (from 6/1/0 to 4/1/0) leads to a lower charge ratio due to the negative

247   charge of CRG sulphate groups. This resulted, as expected, in a zeta potential decrease.

248   Comparing these data with some reported previously for CS/CRG nanoparticles

249   (Grenha et al., 2010), we observe similar tendencies but smaller nanoparticle sizes in the

250   present work for comparable formulations, which might be explained by the use of

251   chitosan and carrageenan from different suppliers (van de Velde, Knutsen, Usov,

252   Rollemay & Cerezo, 2002). In Figure 4B it is seen that the production yields are

253   relatively low (13-19%) and comparable in all cases. In the present study, CS/CRG

254   nanoparticles were used as control.

255   The incorporation of TPP in the matrix of nanoparticles succeeded in providing an

256   effective cross-linking effect. More specifically, the presence of TPP resulted in

257   alterations on all the typical characterization parameters, namely the nanoparticle size

258   and zeta potential (Figure 4A), as well as production yield (Figure 4B). For the highest

259   amount of TPP incorporated (mass ratio of 1 compared to chitosan), particle size

260   decreased to 176-208 nm ($p < 0.05$) and zeta potential also decreased from +80 mV to

261   approximately +50 mV ($p < 0.05$). Size decrease is attributed to the cross-linking effect,

262   which induces the condensation of polymeric chains, resulting in smaller particles. The

263   simultaneous decrease in zeta potential is a consequence, not only of the inclusion of a

264   negatively charged material in the matrix of nanoparticles, but also of the general size

265   decrease, which possibly exposes a lower number of charged groups because of the

266   diminished surface. Interestingly, it can be observed that the incorporation of a mass

267   ratio of only 0.5 of TPP is enough to induce a clear effect on size and zeta potential, but

268   a higher amount of cross-linking agent (mass ratio of 1 compared to chitosan) is

269   necessary to produce a significant effect on production yield ($p < 0.05$). In fact, if the

270   formulation 4/1 is considered as example, it is seen by observation of Figure 4 that the

271   addition of 0.5 TPP does not modify the production yield, but it significantly decreases

272   both the nanoparticles size, by 45% (from 491 nm to 269 nm), and the zeta potential, by

273   25% (from +78 to +54 mV). A further increase of 0.5 TPP, resulting in a final

274   CS/CRG/TPP = 4/1/1, results in a significant increase of the production yield to 36%,

275   while the changes in the size and zeta potential, although significant ($p < 0.05$), are not

276   very pronounced, as size decreases 61 nm and zeta potential 4 mV. This trend was

277   similarly observed for the remaining formulations and, in all cases, the polydispersity

278   index was lower than 0.3. The inclusion of TPP in the nanoparticles was also observed

279   to result in unimodal size distribution.

280   The production yield practically doubled in all formulations with the highest amount

281   of TPP ($p < 0.05$), reaching a maximum of 36% for CS/CRG/TPP = 4/1/1. This

282   behaviour could be explained by the specific mechanism of nanoparticle formation,

283   according to which a determined amount of negative charges is necessary to provide a

284   certain degree of neutralisation of chitosan amino groups, which leads to the formation

285   of nanoparticles. When adding 0.5 TPP the cross-linking occurs, decreasing the size of

286 nanoparticles, but the amount of phosphate groups is not enough to increase the number

287 of formed nanoparticles, an effect that is observed when TPP amount is doubled. The

288 obtained results are in accordance with the ability of TPP to cross-link chitosan,

289 demonstrating in this case the capacity to decrease the size of chitosan-based

290 nanoparticles obtained by polyelectrolyte complexation with another polymer.

291   These results demonstrate, as a whole, that the charge ratio plays a critical role in the

292 production of nanoparticles by electrostatic interactions. In fact, it is shown that the

293 final properties of CS/CRG/TPP nanoparticles can be adjusted by modulating charge

294 ratios.

295

296 **3.2. Nanoparticles stability study**

297   The data corresponding to nanoparticles size evolution over time is depicted in

298 Figure 5, for formulation CS/CRG/TPP = 5/1/1 and for the corresponding CS/CRG

299 formulation, which was used as control. The rationale of conducting this assay in water

300 was the interest in obtaining information on the nanoparticles stability in the

301 resuspension medium. In the cases where the nanoparticles are an intermediate product

302 of the final drug delivery system, as reported in some works of our group (Grenha,

303 Seijo, Serra & Remuñán-López, 2007; Al-Qadi, Grenha & Remuñán-López, 2011), this

304 could avoid the need of extra procedures to stabilize the nanoparticles, as a

305 lyophilization step for instance.

306   The formulation without TPP tends to demonstrate some degree of size variation,

307 although not statistically significant, accompanied by an increase in the polydispersity

308 after 7 days of storage. On the contrary, the formulation containing TPP evidenced

309 improved stability, without signals of significant size variation during the experimental

310 period of 250 days. Zeta potential was also monitored in this study, but no alterations

311 were found over time for either of the assayed formulations (data not shown). Other

312 authors reported the stability of CS/TPP nanoparticles when stored at 5 ºC for 15 days

313 in non-buffered medium, further observing an increase in the polydispersity after that

314 period, as the standard deviation of mean size of the nanoparticles registered a

315 significant increase (López-León, Carvalho, Seijo, Ortega-Vinuesa & Bastos-González,

316 2005). The results found in the present study for the CS/CRG/TPP formulation indicate

317 that TPP acts as a stabiliser, possibly because of its cross-linking effect, which causes

318 polymeric molecules to establish stronger interactions with each other to form a more

319 stable structure, less prone to aggregation. Actually, cross-linking reactions have been

320 described to improve the properties of particulates (Mi, Sung, Shyu, Su & Peng, 2003),

321 hydrogels (Sung, Huang, Chang, Huang & Hsu, 1999) and scaffolds (Adekogbe &

322 Ghanem, 2005), amongst other structures.

323

324 **3.3. Chemical analysis of nanoparticles**

325 As commented above, formulations containing TPP showed different

326 physicochemical characteristic as compared to those without TPP, which suggests that

327 TPP is in fact incorporated in the matrix of nanoparticles. Nevertheless, an indubitable

328 demonstration of TPP presence is possible only by chemical analysis of the

329 formulations. In this manner, specific techniques of chemical analysis, such as FTIR,

330 XPS and TOF-SIMS, were used to characterize the chemical composition of

331 nanoparticles, the last two techniques referring to surface analysis.

332

333 *3.3.1. FTIR analysis*

334 The FTIR spectrum of CS/CRG/TPP nanoparticles is depicted in Figure 6, along with

335 the spectra of all the materials separately (CS, CRG and TPP), which were used as

14

336 controls in this assay. TPP spectrum presents two intense absorption bands at 1147 and

337 906 cm^{-1}, attributed, respectively, to P=O and P-O along with P-O-P. The overlapping

338 of the former with the sulphate band of *k*-carrageenan (van de Velde, Knutsen, Usov,

339 Rollemay & Cerezo, 2002) and of the latter with the carbohydrate bands, renders the

340 detection of their presence in the nanoparticles ambiguous. Moreover, those bands are

341 expected to shift upon protonation and hydrogen bonding (Jiang, Saxena, Song, Ward,

342 Beveridge & Myneni, 2004), which may occur during particle formation. However, the

343 collapse of the sulphate and polysaccharide bands observed in the nanoparticles may be

344 accounted for if TPP is present, especially if shifting of the 1147 cm^{-1} band occurred.

345 Also, the band at 894 cm^{-1} in the nanoparticles may be attributed to a shift in the 906

346 cm^{-1} band of TPP. The amide bands are masked by the 1644 cm^{-1} bending band

347 of adsorbed water (Wilson, Smith, Kacurakova, Saunders, Wellner & Waldron, 2000)

348 and the new 1539 cm^{-1} absorption of the amino groups in protonated CS.

349

350 *3.3.2. Surface analysis by XPS and TOF-SIMS*

351 XPS is one of the most commonly used techniques of surface analysis. Upon

352 exposure of the sample to an X-ray beam, the binding energies of characteristically

353 emitted photoelectrons are measured, providing information on the elements from

354 which they originate, as well as their chemical bonding. Table 1 displays the percentage

355 of each chemical element present in the sample of either controls (CS, CRG and TPP)

356 or nanoparticles. The final chemical composition of a sample can be obtained from core

357 photoemission intensity peak areas using the Shirley background subtraction technique

358 from the survey spectra. The element composition can be quantified by using X-ray

359 photoelectron intensity values and the Scofield theoretically derived set of atomic

360 sensitivity factors. Some of the samples showed an intensive silicon signal (data not

361 shown), which is attributed to the substrate, as a consequence of an incomplete coating

362 of the substrate surface with the sample. These Si signals do not compromise the

363 obtained results and are not included in Table 1. The survey of controls detected the

364 expected elements, such as carbon (C), oxigen (O), nitrogen (N), phosphorus (P) and

365 sulfur (S). The obtained CS composition (64.1% C, 29.6% O and 6.3% N) is similar to

366 that observed by Silva *et al.*, who used the same CS type to produce membranes and

367 obtained 66.4% C, 28.0% O and 5.6% N. In addition, these authors report an O/N ratio

368 of 4.98, which is close to that of the present work (4.69) (Silva et al., 2008).

369   In this work, the prepared nanoparticles were found to contain approximately 57% C,

370 35% O, 4% N, 2% P and 1% S, the content of P being necessarily attributed to the

371 cross-linking agent TPP, and that of S having origin in CRG. The obtained atomic

372 percentages of C, O, N and P were comparable to those reported in other works for the

373 analysis of CS/TPP nanoparticles (53.8% C, 33.8% O, 4.5% N and 2.7% P) (Calvo,

374 Remuñan-López, Vila-Jato & Alonso, 1997b; Grenha, Seijo, Serra & Remuñán-López,

375 2007). The slight variations can be explained by the use of CS of different

376 characteristics and the analysis of nanoparticles with different compositions and mass

377 ratios. The C/N ratio of nanoparticles assayed in the present study (14.3) is slightly

378 higher than those reported by Grenha *et al.* (11.9)(Grenha, Seijo, Serra & Remuñán-

379 López, 2007) and Calvo *et al.* (10.9)(Calvo, Remuñan-López, Vila-Jato & Alonso,

380 1997b). This difference is attributed to the presence of an extra compound in the

381 nanoparticles formulation (CRG), which increased the amount of C, thereby increasing

382 the C/N ratio.

383   Unexpectedly, a certain amount of C and N were detected in the TPP and CRG

384 samples, respectively. This effect was reported by other authors as corresponding to the

385 atmospheric exposure of the samples, which led to the adsorption of some adventitious

16

386   carbon (Barr & Seal, 1995; Swift, 1982) and nitrogen (Allott, Curtis, Hall, Harriman &

387   Battarbee, 1995; Baltrusaitis, Jayaweera & Grassian, 2009; Edwards, Zak, Kellner,

388   Eisenlord & Pregitzer, 2011; Rao, Rao & Ppabhakaran, 1987) on the samples surface.

389   In contrast to photoelectron spectroscopy techniques such as XPS, TOF-SIMS not

390   only provides information on the elements present on analysed surfaces, but also offers

391   detailed molecular information with high sensitivity. This technique has been useful in

392   the characterization of surface chemistry of pharmaceutical systems (Barnes, Kempson

393   & Prestidge, 2011). Figure 7 displays the negative mass spectra, between 50 and 110

394   mass/u, obtained by TOF-SIMS for each of the analysed samples.

395   The spectrum of CS (Figure 7A) evidences a peak at *m/z* 58 corresponding to

396   C_2H_4NO (Al-Qadi, Grenha & Remuñán-López, 2011), as well as peaks at *m/z* 59

397   ($C_2H_3O_2$), 69 (C_3HO_2), and 71 ($C_3H_3O_2$). Typical fragments of chitosan were also

398   detected in the sample of control chitosan, such as $C_{14}H_9NO$, $C_4H_{21}N_{14}O$ and $C_8H_{15}NO_6$

399   (data not shown), the latter representing one of the typical units of chitosan molecule,

400   *N*-acetyl-D-glucosamine (Grenha, Remunan-Lopez, Carvalho & Seijo, 2008; Grenha,

401   Seijo, Serra & Remuñán-López, 2007). The CRG spectrum (Figure 7B) is dominated by

402   SO_2, SO_3 and SO_4H peaks, at *m/z* 64, 80 and 97, respectively. Smaller peaks, attributed

403   to saccharide species, as well as to SO_4, are also present. TPP spectrum (Figure 7C)

404   consists of two peaks, corresponding to PO_2 and PO_3, at *m/z* 63 and 79 (Al-Qadi,

405   Grenha & Remuñán-López, 2011).

406   As it is demonstrated in Figure 7 C and D, the mass spectra of both nanoparticle

407   formulations evidence peaks that are characteristic of all the previous spectra, which

408   correspond to controls. The obtained results are in agreement with those previously

409   observed in the XPS analysis, indicating the presence of all the components (CS, CRG

410   and TPP) in the nanoparticles and suggesting a homogeneous distribution of the various

411 constituents through their matrix. However, given the novelty of this technique, few

412 references were found reporting results of the application of TOF-SIMS on similar

413 materials and those found report fragment peaks with higher masses (mass/u), thus, the

414 establishment of comparisons with previously developed works was very scarce.

415

416 **4. Conclusions**

417 In this work, nanoparticles comprising CS, CRG and TPP were produced and

418 characterized using several techniques such as photon correlation spectroscopy and laser

419 Doppler anemometry, TEM, FTIR, XPS, and TOF-SIMS. The three components were

420 identified in the FTIR, XPS and TOF-SIMS spectra of the nanoparticles, thus indicating

421 an effective association of all the materials. In particular, their detection by the surface

422 analysis techniques suggests a homogeneous distribution through the nanoparticles'

423 matrix.

424 TPP acted as a cross-linker agent and, therefore, enabled the production of

425 nanoparticles with smaller size, apart from increasing their production yield. In

426 addition, the presence of TPP in the nanoparticle matrix increased their stability,

427 providing a shelf-life of at least 9 months. Charge ratios were demonstrated to play a

428 critical role in the nanoparticles formation, since a ratio around 1 leads to precipitation,

429 owing to charge neutralization, while very high charge ratios do not provide enough

430 charges to permit an interaction that induces nanoparticle formation. Overall, it was

431 demonstrated that by modulating charge ratios, the final properties of CS/CRG/TPP

432 nanoparticles can be adjusted to specific applications.

433 Taking into account the small size and high positive charge displayed by the

434 developed nanosystems, they are considered to hold potential for an application in

435 mucosal delivery of macromolecules.

References

Adekogbe, I., & Ghanem, A. (2005). Fabrication and characterization of DTBP-crosslinked chitosan scaffolds for skin tissue engineering. *Biomaterials, 26*(35), 7241-7250.

Al-Qadi, S., Grenha, A., & Remuñán-López, C. (2011). Microspheres loaded with polysaccharide nanoparticles for pulmonary delivery: Preparation, structure and surface analysis. *Carbohydrate Polymers, 86*(1), 25-34.

Allott, T. E. H., Curtis, C. J., Hall, J., Harriman, R., & Battarbee, R. W. (1995). The impact of nitrogen deposition on upland surface waters in Great Britain: A regional assessment of nitrate leaching. *Water, Air, & Soil Pollution, 85*(2), 297-302.

Baltrusaitis, J., Jayaweera, P. M., & Grassian, V. H. (2009). XPS study of nitrogen dioxide adsorption on metal oxide particle surfaces under different environmental conditions. *Physical Chemistry Chemical Physics, 11*(37), 8295-8305.

Barnes, T. J., Kempson, I. M., & Prestidge, C. A. (2011). Surface analysis for compositional, chemical and structural imaging in pharmaceutics with mass spectrometry: A ToF-SIMS perspective. *International Journal of Pharmaceutics, 417*(1-2), 61-69.

460   Barr, T. L., & Seal, S. (1995). Nature of the Use of Adventitious Carbon as a Binding-

461   Energy Standard. *Journal of Vacuum Science & Technology A - Vacuum Surfaces and*

462   *Films, 13*(3), 1239-1246.

463   Bixler, H.J. (1993). The carrageenan connection IV. *British Food Journal, 96*, 12–17.

464   Briggs, D. & Seah, M.P. (1983). *Practical Surface Analysis by Auger and X-Ray*

465   *Photoelectron Spectroscopy*. New York: John Wiley & Sons.

466   Calvo, P., Remuñán-López, C., Vila-Jato, J. L., & Alonso, M. J. (1997a). Novel

467   hydrophilic chitosan-polyethylene oxide nanoparticles as protein carriers. *Journal of*

468   *Applied Polymer Science, 63*(1), 125-132.

469   Calvo, P., Remuñán-López, C., Vila-Jato, J. L., & Alonso, M. J. (1997b). Chitosan and

470   Chitosan/Ethylene Oxide-Propylene Oxide Block Copolymer Nanoparticles as Novel

471   Carriers for Proteins and Vaccines. *Pharmaceutical Research, 14*(10), 1431-1436.

472   Chen, Y., Mohanraj, V. J., Wang, F., & Benson, H. A. E. (2007). Designing chitosan-

473   dextran sulfate nanoparticles using charge ratios. *AAPS PharmSciTech, 8*(4), 131–139.

474   Crouzier, T., Picart, C. (2009). Ion pairing in polyelectrolyte multilayer films containing

475   polysaccharides. *Biomacromolecules, 10*(2), 433-442.

476   de la Fuente, M., Csaba, N., Garcia-Fuentes, M., & Alonso, M. J. (2008). Nanoparticles

477   as protein and gene carriers to mucosal surfaces. *Nanomedicine, 3*(6), 845-857.

478   Desai, M. P., Labhasetwar, V., Amidon, G. L., & Levy, R. J. (1996). Gastrointestinal

479   uptake of biodegradable microparticles: effect of particle size. *Pharmaceutical*

480   *Research, 13*(12), 1838-1845.

481   Dornish, M., Hagen, A., Hansson, E., Peucheur, C., Vedier, F., & Skaugrud, O. (1997).

482   *Safety of Protasan™: Ultrapure chitosan salts for biomedical and pharmaceutical use*.

483   Lyon: Jacques Andre publisher.

484   Edwards, I. P., Zak, D. R., Kellner, H., Eisenlord, S. D., & Pregitzer, K. S. (2011).

485   Simulated Atmospheric N Deposition Alters Fungal Community Composition and

486   Suppresses Ligninolytic Gene Expression in a Northern Hardwood Forest. *Plos One,*

487   *6*(6), e20421.

488   Fernández-Urrusuno, R., Calvo, P., Remuñán-López, C., Vila-Jato, J. L., & José

489   Alonso, M. (1999). Enhancement of Nasal Absorption of Insulin Using Chitosan

490   Nanoparticles. *Pharmaceutical Research, 16*(10), 1576-1581.

491   Grenha, A. (2012). Chitosan nanoparticles: a survey of preparation methods. *Journal of*

492   *Drug Targeting,* doi: 10.3109/1061186X.2011.654121.

493   Grenha, A., Gomes, M. E., Rodrigues, M., Santo, V. E., Mano, J. F., Neves, N. M., &

494   Reis, R. L. (2010). Development of new chitosan/carrageenan nanoparticles for drug

495   delivery applycations. *Journal of Biomedical Materials Research Part A, 92A*, 1265-

496   1272.

497   Grenha, A., Remuñán-López, C., Carvalho, E. L., & Seijo, B. (2008). Microspheres

498   containing lipid/chitosan nanoparticles complexes for pulmonary delivery of therapeutic

499   proteins. *European Journal of Pharmaceutics and Biopharmaceutics, 69*(1), 83-93.

500   Grenha, A., Seijo, B., Serra, C., & Remuñán-López, C. (2007). Chitosan Nanoparticle-

501   Loaded Mannitol Microspheres: Structure and Surface Characterization.

502   *Biomacromolecules, 8*(7), 2072-2079.

503 Hirano, S., Seino, H., Akiyama, Y., & Nonaka, I. (1988). Biocompatibility of chitosan

504 by oral and intravenous administrations. *Polymer Materials and Science Engineering,*

505 *59,* 897-901.

506 Janes, K. A., Calvo, P., & Alonso, M. J. (2001). Polysaccharide colloidal particles as

507 delivery systems for macromolecules. *Advanced Drug Delivery Reviews, 47*(1), 83-97.

508 Jani, P., Halbert, G. W., Langridge, J., & Florence, A. T. (1990). Nanoparticle Uptake

509 by the Rat Gastrointestinal Mucosa: Quantitation and Particle Size Dependency.

510 *Journal of Pharmacy and Pharmacology, 42*(12), 821-826.

511 Jiang, W., Saxena, A., Song, B., Ward, B. B., Beveridge, T. J., & Myneni, S. C. B.

512 (2004). Elucidation of functional groups on Gram-positive and Gram-negative bacterial

513 surfaces using infrared spectroscopy. *Langmuir, 20,* 11433-11442.

514 Lehr, C. M., Bouwstra, J. A., Schacht, E. H., & Junginger, H. E. (1992). In vitro

515 evaluation of mucoadhesive properties of chitosan and some other natural polymers.

516 *International Journal of Pharmaceutics, 78*(1-3), 43-48.

517 Lim, Y. M., Gwon, H. J., Choi, J. H., Shin, J., & Nho, Y. C. (2010). Preparation and

518 Biocompatibility Study of Gelatin/Kappa-carrageenan Scaffolds. *Macromolecular*

519 *Research, 18,* 29-34.

520 Liu, Z., Jiao, Y., Wang, Y., Zhou, C., & Zhang, Z. (2008). Polysaccharides-based

521 nanoparticles as drug delivery systems. *Advanced Drug Delivery Reviews, 60,* 1650–

522 1662.

523 López-León, T., Carvalho, E. L. S., Seijo, B., Ortega-Vinuesa, J. L., & Bastos-

524 González, D. (2005). Physicochemical characterization of chitosan

525 nanoparticles:electrokinetic and stability behavior. *Journal of Colloid and Interface*

526 *Science, 283,* 344–351.

527   Ma, O., Lavertu, M., Sun, J., Nguyen, S., Buschmann, M. D., Winnik & F. M.,

528   Hoemann, C. D. (2008). Precise derivatization of structurally distinct chitosans with

529   rhodamine B isothiocyanate, *Carbohydrate Polymers*, *72*, 616–624.

530   Malafaya, B. M., Silva, A. G., & Reis, R. L. (2007). Natural-origin polymers as carriers

531   and scaffolds for biomolecules and cell delivery in tissue engineering applications.

532   *Advanced Drug Delivery Reviews, 59*, 207-233.

533   Mi, F. L., Sung, H. W., Shyu, S. S., Su, C. C., & Peng, C. K. (2003). Synthesis and

534   characterization of biodegradable TPP/genipin co-crosslinked chitosan gel beads.

535   *Polymer, 44*(21), 6521-6530.

536   Mohamadnia, Z., Zohuriaan-Mehr, M. J., Kabiri, K., Jamshidi, A., & Mobedi, H.

537   (2007). pH-Sensitive IPN Hydrogel Beads of Carrageenan-Alginate for Controlled Drug

538   Delivery. *Journal of Bioactive and Compatible Polymers, 22*, 342-356.

539   Mohanraj, V. J., & Chen, Y. (2006). Nanoparticles – A Review. *Tropical Journal of*

540   *Pharmaceutical Research, 5*, 561-573.

541   Nizri, G., Magdassi, S., Schmidt, J., Cohen, Y., & Talmon, Y. (2004). Microstructural

542   Characterization of Micro- and Nanoparticles Formed by Polymer−Surfactant

543   Interactions. *Langmuir, 20*(11), 4380-4385.

544   Nizri, G., Makarsky, A., Magdassi, S., & Talmon, Y. (2009). Nanostructures Formed by

545   Self-Assembly of Negatively Charged Polymer and Cationic Surfactants. *Langmuir,*

546   *25*(4), 1980-1985.

547   Rao, C. N. R., Rao, G. R., & Ppabhakaran, K. (1987). A combined XPS-UPS-EELS

548   study of nitrogen adsorbed on clean and barium-promoted iron surfaces: The nature of

549   the precursor to dissociation. *Chemical Physics Letters, 134*(1), 47-50.

550   Rawat, M., Singh, D., & Saraf, S. (2006). Nanocarriers: promising vehicle for bioactive

551   drugs. *Biological & Pharmaceutical Bulletin, 29*(9), 1790-1798.

552   Reis, C., & Ribeiro, A. (2006). Nanoencapsolation II. Biomedical applications and

553   current status of peptide and protein nanoparticulate delivery systems. *Nanomedicine:*

554   *Nanotechnology, Biology and Medicine, 2*, 53-65.

555   Saboktakin, M. R., Tabatabaie, R. M., Maharramov, A., & Ramazanov, M. A. (2010).

556   Synthesis and characterization of superparamagnetic chitosan–dextran sulphate

557   hydrogels as nano carriers for colon-specific drug delivery. *Carbohydrate Polymers, 81*,

558   372-376.

559   Silva, S. S., Luna, S. M., Gomes, M. E., Benesch, J., Pashkuleva, I., Mano, J. F., &

560   Reis, R. L. (2008). Plasma Surface Modification of Chitosan Membranes:

561   Characterization and Preliminary Cell Response Studies. *Macromolecular Bioscience,*

562   *8*(6), 568-576.

563   Sung, H. W., Huang, D. M., Chang, W. H., Huang, R. N., & Hsu, J. C. (1999).

564   Evaluation of gelatin hydrogel crosslinked with various crosslinking agents as

565   bioadhesives: In vitro study. *Journal of Biomedical Materials Research, 46*(4), 520-530.

566   Swift, P. (1982). Adventitious Carbon - the Panacea for Energy Referencing. *Surface*

567   *and Interface Analysis, 4*(2), 47-51.

568   van de Velde, F., Knutsen, S. H., Usov, A. I., Rollemay, H. S., & Cerezo, A. S. (2002).

569   1H and13C high resolution NMR spectroscopy of carrageenans:application, research

570   and industry. *Trends in Food Science & Technology, 13*, 73–92.

571   Wilson, R. H., Smith, A. C., Kacurakova, M., Saunders, P. K., Wellner, N., & Waldron,

572   K. W. (2000). The mechanical properties and molecular dynamics of plant cell wall

573 polysaccharides studied by Fourier-transform infrared spectroscopy. *Plant Physiology,*

574 *124*(1), 397-405.

575

Table 1

Table 1 - Surface composition (atomic percentage) determined by XPS of CS, CRG, TPP and CS/CRG/TPP nanoparticles of different ratios.

Element	CS (%)	CRG (%)	TPP (%)	4/1/1 NP (%)	5/1/1 NP (%)
C	64.1	57.4	16.0	57.5	57.9
O	29.6	38.2	63.6	35.2	35.1
N	6.3	1.1	0	4.0	4.0
P	0	0	20.4	2.0	1.7
S	0	3.3	0	1.3	1.3
Ratio O/N	4.69	35.7	0	8.75	8.73
Ratio C/N	10.2	53.6	0	14.3	14.4

CS: Chitosan, CRG: Carrageenan; NP: Nanoparticles; TPP: Tripolyphosphate

Figure captions

Fig. 1. Chemical structures of materials composing the matrix of nanoparticles: chitosan, *k*-carrageenan and sodium tripolyphosphate.

Fig. 2. TEM microphotograph of representative CS/CRG/TPP (4/1/1) nanoparticles.

Fig. 3. Representative scheme of A) positive/negative charge ratio of each formulation (white fill: formation of nanoparticles; dark grey: precipitation; light grey: inability to form nanoparticles); B) the ability to form nanoparticles according to formulation composition: precipitation (□); nanoparticles (●); solution (◊).

Fig. 4. Effect of CS/CRG mass ratio and TPP amount on **A)** nanoparticle size (round marks) and zeta potential (triangular marks) and **B)** production yield of nanoparticle (square marks). White: 0 TPP; grey: 0.5 TPP; black: 1 TPP (mean ± SD, $n = 3$).

Fig. 5. Evolution of CS/CRG (○) and CS/CRG/TPP (●) nanoparticle size as a function of time, upon storage at 4 ºC (mean ± SD, $n = 3$).
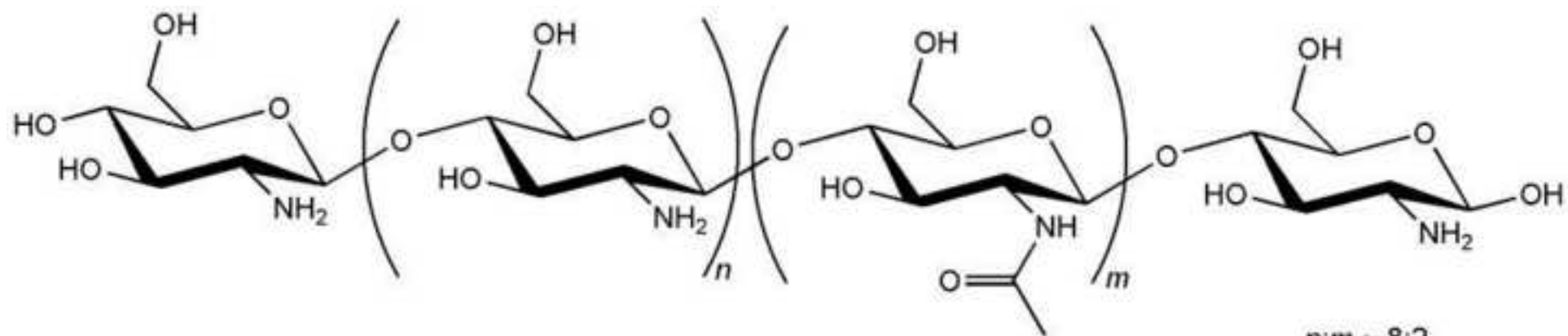
Fig. 6. FTIR spectra of CS, CRG, TPP and CS/CRG/TPP (5/1/1) nanoparticles.

Fig. 7. Negative ion mass spectra obtained by TOF-SIMS analysis of (A) CS, (B) CRG, (C) TPP, (D) CS/CRG/TPP = 4/1/1 nanoparticles and (E) CS/CRG/TPP = 5/1/1 nanoparticles.
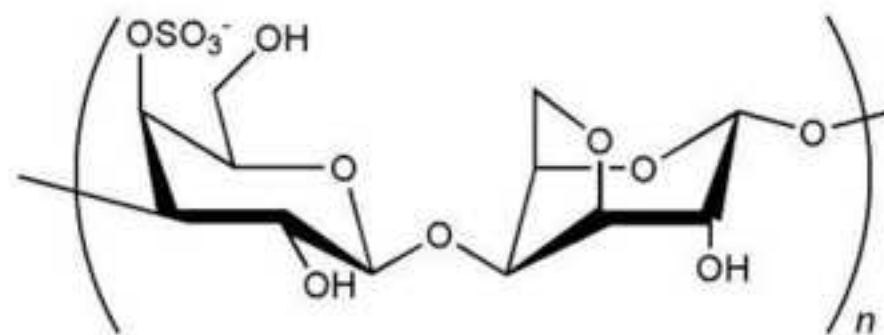
Figure 1
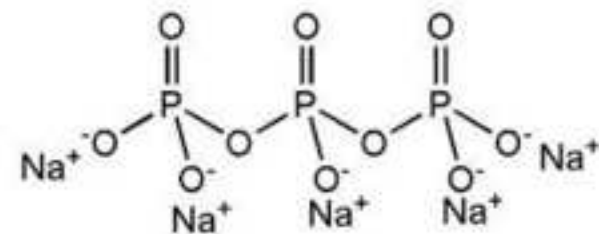[Click here to download high resolution image](#)

Chitosan (CS)

$n:m \approx 8:2$

k-Carrageenan (CRG)

Sodium tripolyphosphate (TPP)

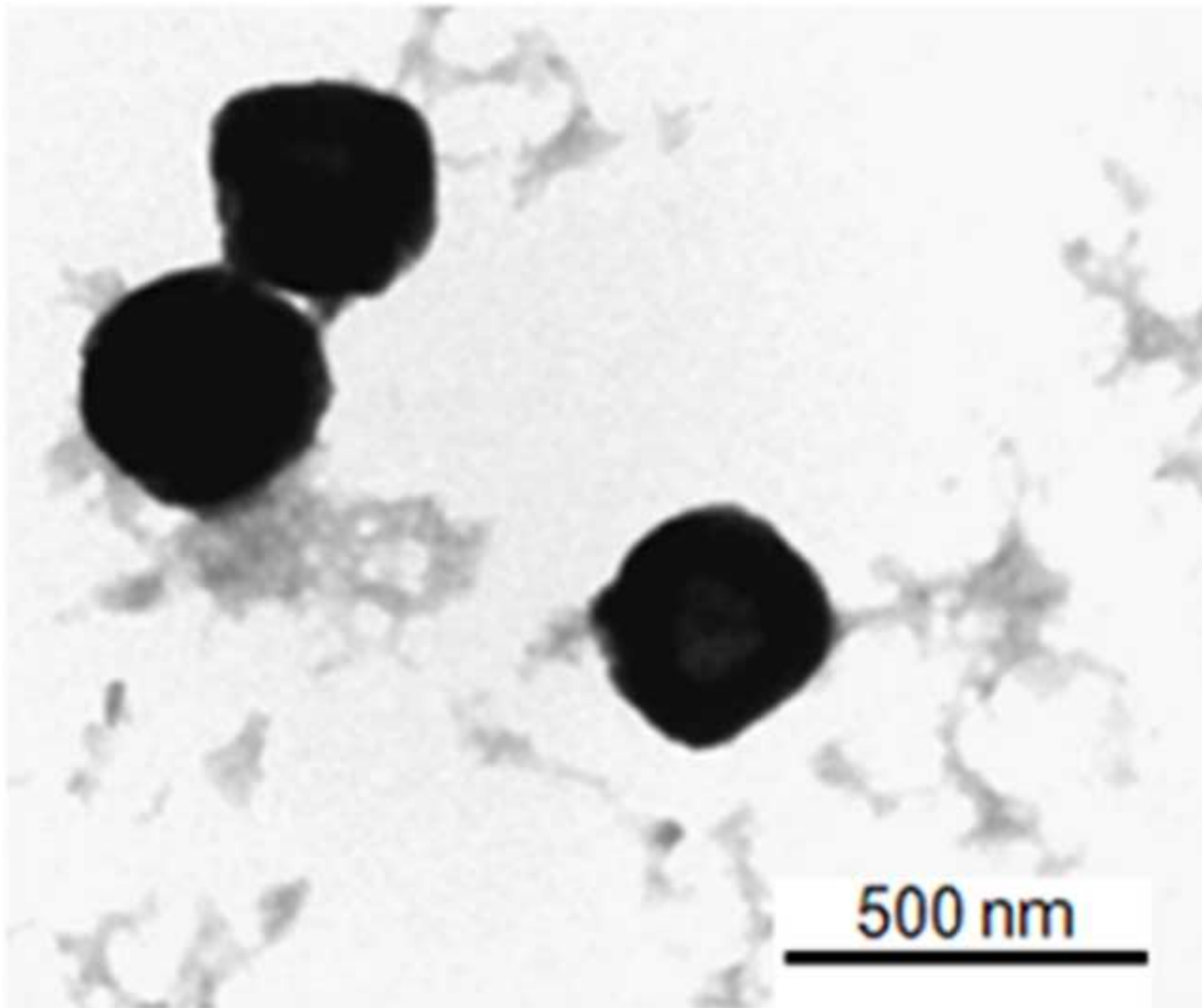**Figure 2**
Click here to download high resolution image

500 nm

Figure 3
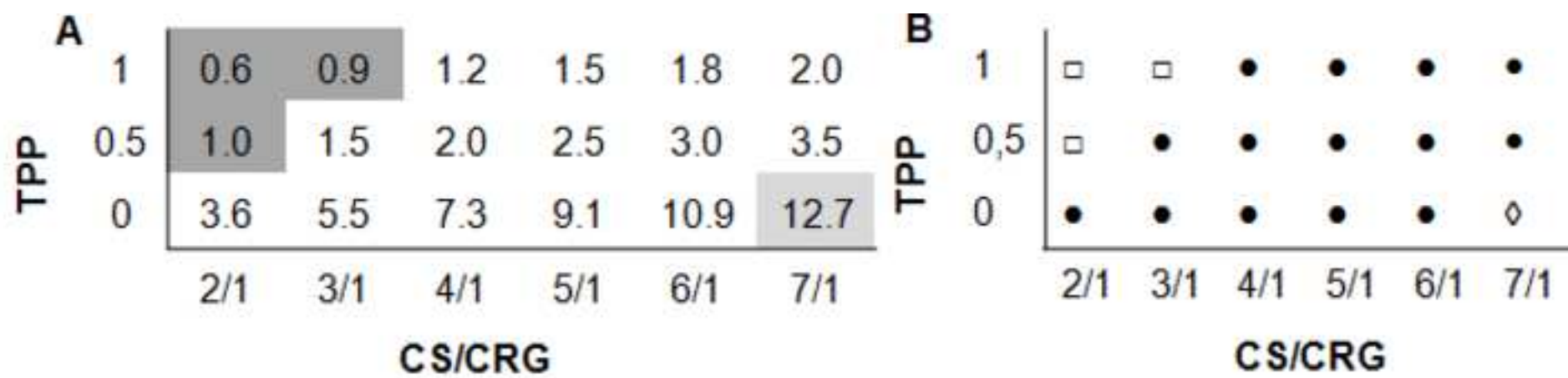**Click here to download high resolution image**

A

TPP							
1	0.6	0.9	1.2	1.5	1.8	2.0
0.5	1.0	1.5	2.0	2.5	3.0	3.5
0	3.6	5.5	7.3	9.1	10.9	12.7
	2/1	3/1	4/1	5/1	6/1	7/1

CS/CRG

B

CS/CRG

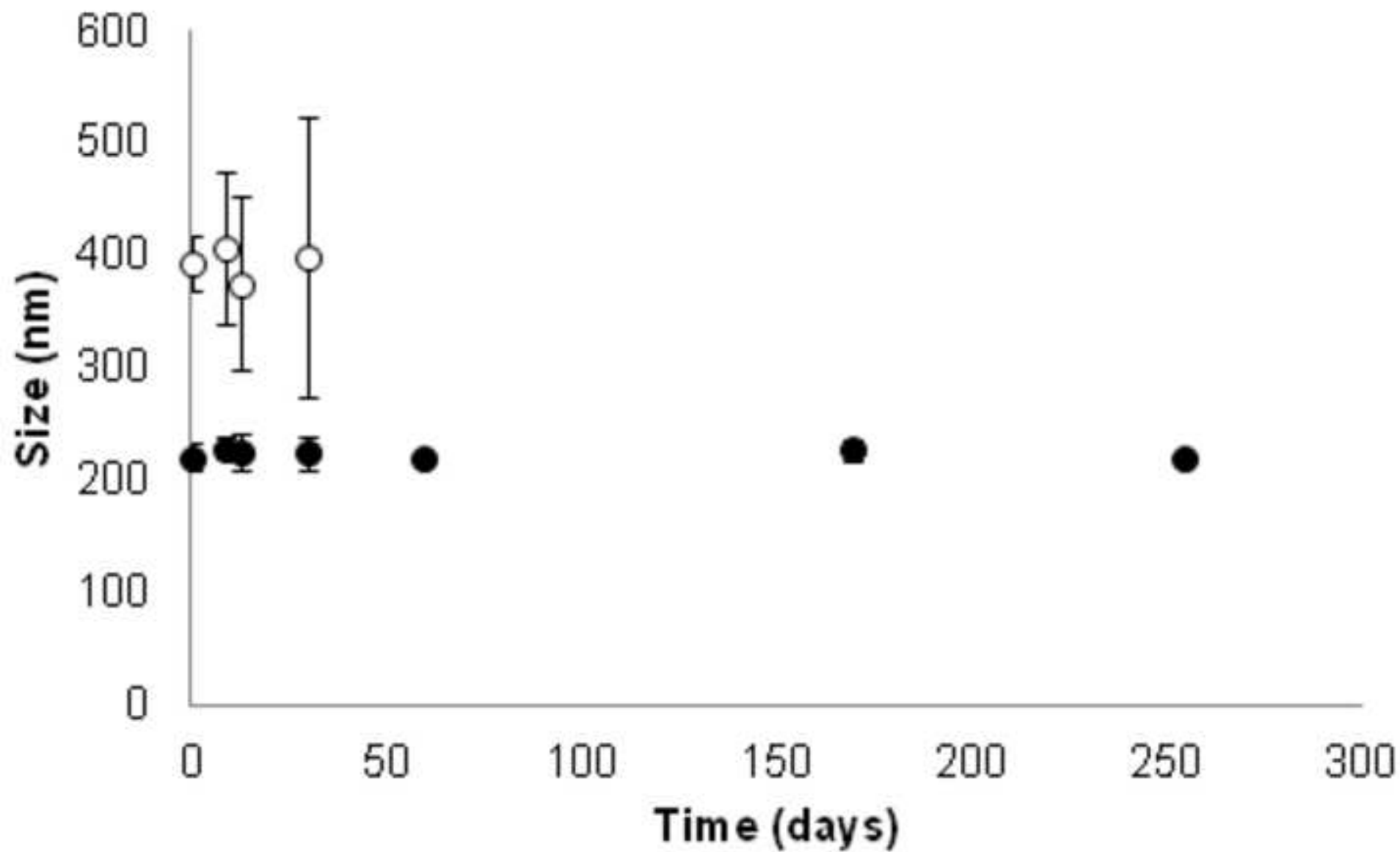**Figure 4**
Click here to download high resolution image
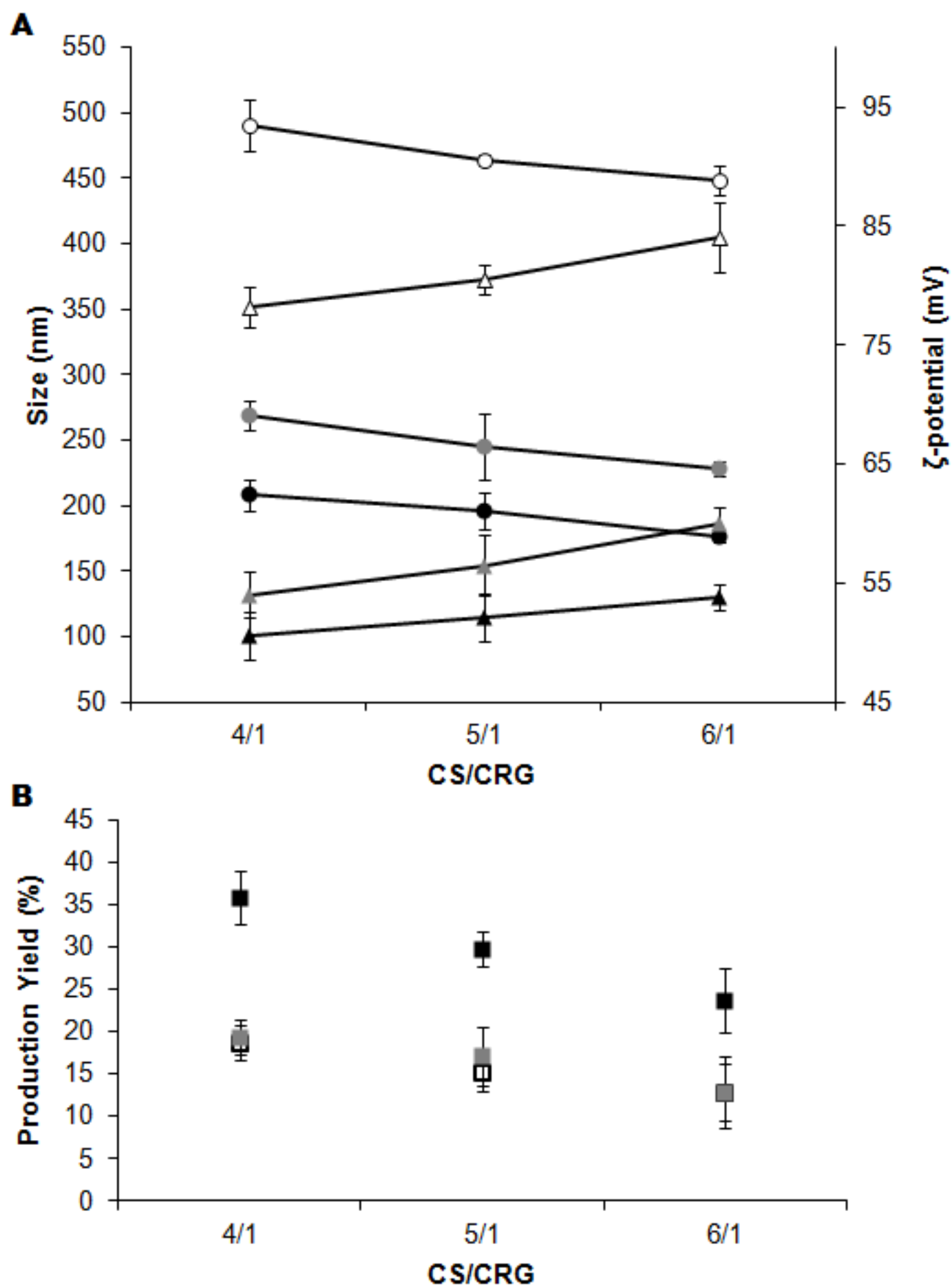
Figure 5
Click here to download high resolution image

Chitosan (CS)

Amide I
Amide II
1652 1594
Glycosidic linkage
1080

k-Carrageenan (CRG)

1647
Sulphate
Glycosidic linkage
3,6-Anhydrogalactose
Galactose-4-sulphate
846
929
1262
1069

Tripolyphosphate (TPP)

906
1147

Ammonium
1539
1644
1226
1156
849
894
931
1072

CS/kCRG/TPP
nanoparticles

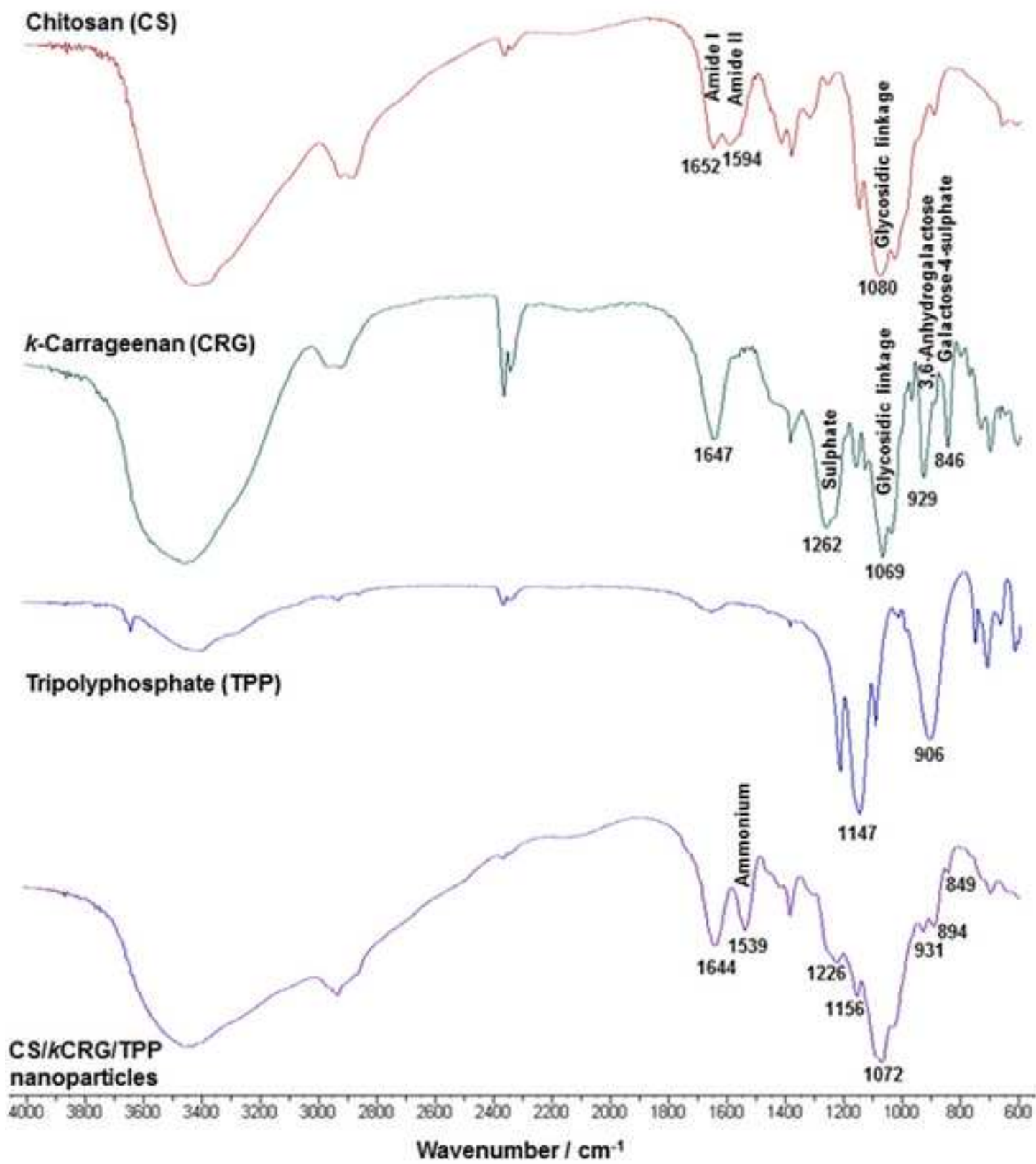4000 3800 3600 3400 3200 3000 2800 2600 2400 2200 2000 1800 1600 1400 1200 1000 800 600

Wavenumber / cm⁻¹

Figure 7
Click here to download high resolution image

Figure 7